

# Gaussian Mask Convolution for Convolutional Neural Networks

Qi Chen, Chao Li, Jia Ning, Kun He<sup>†</sup>

School of Computer Science and Technology  
Huazhong University of Science and Technology

{bloom24, D201880880, ninja, brooklet60}@hust.edu.cn

## Abstract

Square convolution is a default unit in convolutional neural networks as it fits well on the tensor computation for convolution operation, which usually has a fixed  $N \times N$  receptive field (RF). However, what matters most to the network is the effective receptive field (ERF), which indicates the extent each pixel contributes to the output. ERF shows a Gaussian distribution and can not be modeled by simply sampling pixels with offsets. To simulate ERF, we propose a Gaussian Mask convolutional kernel (GMConv) in this work. Specifically, GMConv utilizes the Gaussian function to generate a concentric symmetry mask and put the mask over the kernel to refine the RF. Our GMConv can directly replace the standard convolutions in existing CNNs and can be easily trained end-to-end by standard back-propagation. Extensive experiments on multiple image classification benchmark datasets show that our method is comparable to, and outperforms in many cases, the standard convolution. For instance, using GMConv for AlexNet and ResNet-50, the top-1 accuracy on ImageNet classification is boosted by 0.98% and 0.85%, respectively.

## 1. Introduction

Convolutional Neural Networks (CNNs) have significantly boosted the performance of vision tasks, including image classification [10, 17], object detection [8, 28], and many other applications [23, 33]. It was not until recent years that Vision Transformers (ViTs) [6, 20, 21, 37] surpassed CNN in computer vision and took the place of CNNs as the mainstream research but needs a cumbersome amount of computational resources.

Meanwhile, there are still many excellent works devoted to the CNN design. The recently proposed large kernel CNNs [5, 19, 22] show that these pure CNN architectures are competitive with state-of-the-art ViTs in accuracy, scalabil-

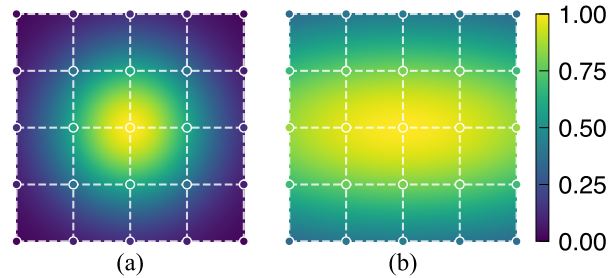


Figure 1. Typical receptive fields of  $5 \times 5$  Gaussian mask convolutions. (a) Receptive field of GMConv with circular mask. (b) Receptive field of GMConv with elliptic mask.

ity, and robustness across all major benchmarks. All these efforts try to draw attention to CNN again and let the literature reconsider the importance of convolutions for computer vision. On the other hand, square convolutions have long been used as the standard structure to build various CNN architectures [10, 13, 27, 35, 39] as it fits nicely with the rectangular geometry of matrices and tensor computation. Although there have been some works on designing new convolutional kernels by sampling pixels with offsets in recent years [3, 9, 15, 41], they are relatively few in comparison to the CNN architecture design.

The receptive field (RF) is a basic concept in CNNs, which means the region in the input where a CNN unit depends. The research of Luo *et al.* [24] further introduces the concept of effective receptive field (ERF), indicating an effective area within the receptive field that primarily influences the response of an output unit. They emphasize that the ERF, which shows how much each pixel contributes to the output, is what really matters to the network. The ERF can not be modeled by simply sampling pixels with offsets. So we aim to simulate it from a different perspective.

Inspired by the fact that the ERF exhibits a Gaussian distribution, we propose a Gaussian Mask Convolutional Kernel (GMConv) to introduce a circular (or elliptic) concentric RF into the CNN kernels. It adds  $\sigma$  ( $\sigma_1, \sigma_2$ ) parameters in

the standard convolution and generates the RF adjustment mask by a Gaussian-like function. Different from existing related works [3, 15, 41] that focus on the shapes of convolutional kernel design, we focus on adding masks on the square kernels to change the convolution operation. The effect of our GMConv is illustrated in Figure 1. As the parameters vary, the RFs of GMConv show a progressive circular (elliptical) concentric distribution, which could approximate effective receptive fields.

Specifically, we introduce two kinds of GMConv. The first is the static version of GMConv (S-GMConv), which has only one more parameter ( $\sigma$ ) compared to the standard convolution. According to the parameter, convolutions can generate the corresponding circular RF mask. It enables the convolutions to model spatial relationships and RF adjustment. The second is the dynamic version of GMConv (D-GMConv), which further strengthens GMConv with more parameters that control the mask distribution from both horizontal and vertical aspects, and the dynamic sigma module, which predicts specialized sigma parameters dynamically for each input. Both modules are lightweight and can be easily used as a drop-in replacement for convolutions in CNNs.

Extensive experiments demonstrate that by replacing standard convolution with GMConv, we can considerably boost the performance of equivalent networks on CIFAR-10, CIFAR-100 [16] and ImageNet [11]. In addition, we find that the concentric RF can enhance the model’s robustness to rotational distortions. Finally, our visualization shows that GMConv generally affects the shallow layers of the networks and helps the networks to locate the target objects more accurately and integrally. Our main contributions are three-fold:

- We propose GMConv, a simple yet effective convolution, that generates a Gaussian distribution mask to introduce concentric circular (elliptic) receptive fields to the CNN kernels.
- We design the static and dynamic version of GMConv, which can be easily integrated with commonly used CNN architectures with negligible extra parameters and complexity.
- Thorough experiments are conducted to demonstrate that GMConv can improve the performance of multiple common benchmark models on the three benchmark datasets, CIFAR-10, CIFAR-100, and ImageNet.

## 2. Related Work

### 2.1. CNN Structure Design

Since AlexNet [17] revealed the potential of CNNs, there are numerous emerging powerful manually designed networks [10, 13, 32, 39] and automatic architectures [27, 36]. Most of these network structures are divided into three por-

tions: stem, body, and head [27]. In general, the network stem is an  $N \times N$  convolution with stride two that halves the height and width of an input image. The network head setting is based on the concrete task, *e.g.*, a global average pooling followed by a fully connected layer for predicting the output class in the image classification task. The network body consists of multiple stages of transformation at progressively reduced resolution. Generally, the stem and head are kept fixed and simple, and most works are focused on the structure of the network body, which is more critical to network computation and accuracy. Based on the design pattern, when applying GMConv into CNN, we use different versions of GMConv for the stem layer and the body layer. The details are discussed subsequently in Section 3.

### 2.2. Convolutional Kernel Design

Grouped convolutions [17] divide the feature maps to multiple GPUs to process respectively and finally fuse the results, which have inspired the design of follow-up lightweight networks. Depthwise separable convolutions [2, 12] consist of a depthwise convolution followed by a pointwise convolution. The depthwise convolution first performs a spatial grouped convolution independently over each channel of the input. Then the pointwise convolution applies a  $1 \times 1$  convolution to fuse the channel outputs of the depthwise convolution. This approach achieves a good trade-off between accuracy and resource, and is widely used in lightweight computing devices.

The above variants inherit the square kernel in general, thus resulting in a fixed receptive field. To enable more flexible receptive fields and better learn the spatial transformation from the input, another line of studies [3, 15, 41] designs more free-form deformation convolutions. Active convolutions [15] and deformable convolutions [3, 41] augment the sampling locations in the receptive fields with dynamic offsets that are learned from the preceding features via additional convolution layers. Deformable ConvNets v2 [41] further introduces a dynamic modulation mechanism that evaluates the importance of each sampled location but with higher computation overhead. Deformable Kernel [7] re-samples the original kernel space towards recovering the deformation of objects. In contrast, our focus is transforming the receptive field inside the original kernel. It gives convolutions more flexible receptive fields without changing the tensor computation for the standard convolutions.

There are also some works using masked convolutions [14, 18, 25]. The MaConv [25] and LMConv [14] use binary masks to generative models. The Noise2void [18] employs a binary mask for denoising. In contrast, GMConv applies a Gaussian-like mask to model the effective receptive field for the image classification task.

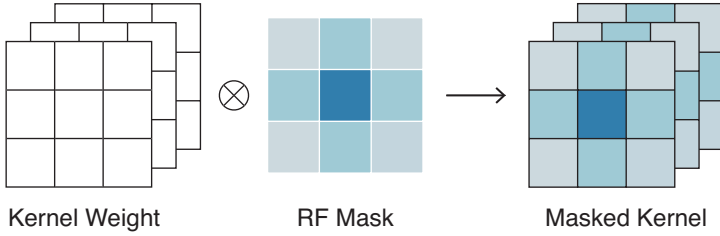


Figure 2. Overview of the GMConv.

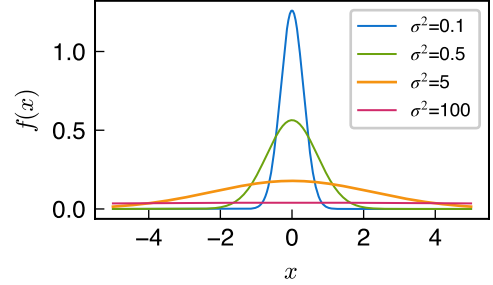


Figure 3. Curves of standard one-dimensional Gaussian function. All  $\mu$  values are set to 0 for comparisons.

### 2.3. Dynamic Mechanism

The dynamic mechanism has promoted many tasks to new state-of-the-art. Benefiting from input-dependency characteristic, networks can adjust themselves to fit the diverse inputs automatically and improve the representation ability. From the perspective of dynamic features, SE-Net [13] proposes the ‘‘Squeeze-and-Excitation’’ block, which adaptively recalibrates channel-wise features by explicitly modeling the interdependencies among channels. The subsequent proposed CBAM block [38] recalibrates both channel-wise and spatial-wise features. From the aspect of dynamic convolution kernels, the deformable convolutions [3, 15, 41] learn offsets for each input to enable adaptive geometric variations. CondConv [40] and Dynamic Convolution [1] dynamically aggregate multiple parallel convolution kernels to increase the model capacity. Different from the above methods, D-GMConv applies a dynamic RF mask over the kernel to enable adaptive RF on square convolutions.

### 2.4. Gaussian-Distributed Effective Receptive Field

Luo *et al.* [24] find that the effective receptive field, which shows main contributions to the unit’s output, only occupies a small fraction of the actual RF and exhibits a Gaussian distribution. This finding has inspired works that incorporate the Gaussian distribution to convolutions. In image segmentation, the work of Shelhamer *et al.* [31] and Sun *et al.* [34] use Gaussian distribution to construct the deformable convolutions. They generally follow the line of learning offsets for geometric variations.

## 3. Gaussian Mask Convolution

In this section, we introduce the details of GMConv. First, we describe the overview of GMConv. Then, we illustrate how to generate the RF masks. Next, we propose the static GMConv and dynamic GMConv. Finally, we describe the detail of applying GMConv to CNN architectures.

**Overview of GMConv.** Given a standard square convolutional kernel  $\mathbf{W} \in \mathbb{R}^{K \times K}$  and the corresponding receptive field  $\mathbf{I}_j \in \mathbb{R}^{K \times K}$  centered on the location  $j$ . Let  $\hat{\mathbf{I}}_j \in \mathbb{R}^{K^2 \times 1}$  and  $\hat{\mathbf{W}} \in \mathbb{R}^{K^2 \times 1}$  represent the resized (from  $K \times K$  to  $K^2 \times 1$ ) RF and the kernel weight. Then the corresponding output can be expressed as  $\mathbf{O}_j = \hat{\mathbf{W}}^\top \hat{\mathbf{I}}_j$ .

In our GMConv, we place a mask  $\mathbf{M}_g \in \mathbb{R}^{K \times K}$  between the input and the kernel. The mask has a concentric distribution, which affects kernel’s perception toward different regions. Then the convolution can be expressed as:

$$\mathbf{O}_j = \hat{\mathbf{W}}^\top (\hat{\mathbf{M}}_g \cdot \hat{\mathbf{I}}_j) = (\hat{\mathbf{W}}^\top \cdot \hat{\mathbf{M}}_g^\top) \hat{\mathbf{I}}_j, \quad (1)$$

where  $\hat{\mathbf{M}}_g \in \mathbb{R}^{K^2 \times 1}$  represents the resized RF mask of  $\mathbf{M}_g$ . In this way, we can directly apply  $\mathbf{M}_g$  to the kernel instead of the RF. Due to sliding windows, RFs are keeping changing. So employing  $\mathbf{M}_g$  to kernels is straightforward and efficient. As shown in Figure 2, the overall process can be simplified as:

$$\mathbf{W}' = \mathbf{W} \otimes \mathbf{M}_g, \quad (2)$$

where  $\otimes$  indicates Hadamard multiplication,  $\mathbf{W}' \in \mathbb{R}^{C \times K \times K}$  denotes the final RF refined kernel. The mask values are broadcasted along the channel dimension during multiplication. Details of GMConv are described below.

**Circular Gaussian Mask.** We design the circular concentric Gaussian mask based on the one-dimensional (1D) Gaussian function:

$$f_{1D}(d) = A \exp\left(-\frac{(d - \mu)^2}{2\sigma^2}\right), \quad (3)$$

where  $A = (\sqrt{2\pi}\sigma)^{-1}$  represents the coefficient terms,  $d$  denotes the distance between points and the center  $\mu$  within the sample grids, the parameter  $\sigma$  determines the distribution of the mask,  $\mu$  denotes the extreme point, where the function takes on the highest value. In particular, we put  $\mu$  on the center of the convolutional kernel.

To avoid the appearance of extreme values and absence of the receptive fields, we perform *Max* normalization over the mask:

$$G_{1D}(d) = \frac{f_{1d}(d)}{\max_{d \in D} f_{1d}(d)}, \quad (4)$$

where  $D$  indicates a set of distances from the center of the kernel. We visualize the 1D Gaussian function in Figure 3 to illustrate the potential risk if directly applying the function. We can observe that when the  $\sigma^2$  values are too large, the curve becomes very flat, and every point on the curve tends to 0; the corresponding mask will make the kernel lose the overall receptive field. On the other hand, as the  $\sigma^2$  goes to zero, the curve becomes very sharp, its peak tends to infinity, and the points around tend to zero. In this way, the convolutional kernel can only perceive the center point. However, it may lead to the occurrence of a maximum value, which is not a favorable property. With *Max* normalization, the modified Gaussian function always obtains the maximum value of 1 at the center point, thus avoiding the appearance of extreme values and the absence of receptive fields.

**Elliptical Gaussian Mask.** We design the generation function for the elliptical concentric Gaussian mask with two-dimensional Gaussian functions. The *Max* normalization is also employed to avoid extreme values and the absence of receptive fields:

$$f_{2D}(x, y) = A' \exp \left[ -\frac{1}{2} \left( \frac{(x - \mu_1)^2}{\sigma_1^2} + \frac{(y - \mu_2)^2}{\sigma_2^2} \right) \right], \quad (5)$$

$$G_{2D}(x, y) = \frac{f_{2D}(x, y)}{\max_{x, y \in K} f_{2D}(x, y)}, \quad (6)$$

where  $A' = (2\pi\sigma_1\sigma_2)^{-1}$  represents the coefficient term, and parameters  $\sigma_1, \sigma_2$  determine the distribution of the mask,  $(\mu_1, \mu_2)$  denotes the extreme point,  $(x, y)$  denotes the offset from the center of the convolutional kernel, and  $K$  represents a set of offsets within the kernel's view.

**Static GMConv.** We then apply the 1D generate function in Eq. (3) and Eq. (4) to generate a Gaussian RF mask. Therefore, apart from learning the network weights, static GMConv only needs to learn one additional  $\sigma$  parameter, which is initialized to 5 by default. After training, we integrate the mask into the kernel weights. As a result, it introduces NO extra inference-time computational overhead compared to the standard convolution.

**Dynamic GMConv.** In dynamic GMConv, we apply the 2D generation function to generate the RF mask as illustrated in Figure 4. The parameters  $\sigma_1, \sigma_2$  are computed by the dynamic sigma module as shown in Figure 5. Following the squeeze-and-excitation pattern, we first squeeze global information of a feature map  $x \in \mathbb{R}^{C \times H \times W}$  by using both global-max-pooling and global-average-pooling operations,

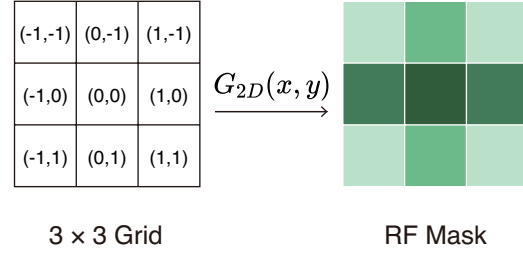


Figure 4. Illustration of the mask generation with two-dimensional Gaussian-like function.

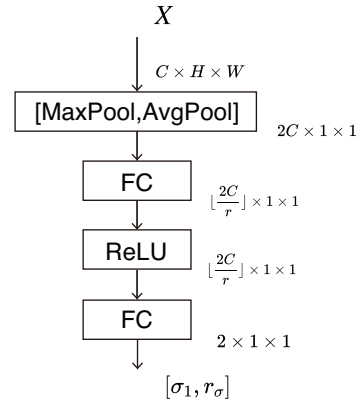


Figure 5. Diagram of the learnable sigma module.

generating two different context vectors:  $x_{max} \in \mathbb{R}^C$  and  $x_{avg} \in \mathbb{R}^C$ . Then we concatenate the two vectors as the global context descriptor:  $z = Concat(x_{max}, x_{avg})$ . Next, the descriptor  $z$  is forwarded to two fully connected layers (with a ReLU in-between) and outputs the value of  $\sigma_1$  and the ratio of  $\sigma_2$  to  $\sigma_1, r_\sigma$ . The overall process is summarized as follows:

$$F_\sigma(z) = \mathbf{W}_1 \cdot ReLU(\mathbf{W}_0 \cdot z) + \mathbf{B}_1, \quad (7)$$

where  $z \in \mathbb{R}^{2C}$ ,  $\mathbf{W}_0 \in \mathbb{R}^{\lfloor 2C/r \rfloor \times 2C}$  refers to the weights of the first fully connected layers,  $\mathbf{W}_1 \in \mathbb{R}^{2 \times \lfloor 2C/r \rfloor}$  and  $\mathbf{B}_1 \in \mathbb{R}^2$  refer to the weights and bias of the second fully connected layers, respectively,  $r$  is the reduction ratio (which is set to 4/3 by default).

**Applying GMConv to CNNs.** Our GMConv can be readily applied to existing CNNs and be easily trained end-to-end by standard back-propagation. When applying GMConv to CNNs, we replace convolutions in stem with dynamic GMConv and convolutions in body with static GMConv. The configurations are based on the following considerations. First, using too much D-GMConv would make

the network too hard to be trained, as they require joint optimization of all kernel weights and the dynamic sigma modules across multiple layers. Second, D-GMConv would introduce more parameters and complexity to networks. Finally, in CNN architecture designs, the stem layer is usually kept concise, and most works are concerned with the structure of the network body. So in relatively complex architectures, the convolutional kernel should be kept as simple as possible, while for many simple structures, we can try to enhance it with more complex convolutions.

## 4. Experiments and Discussions

In this section, we empirically demonstrate the effectiveness of GMConv on the standard image classification datasets, CIFAR-10, CIFAR-100 [16], and ImageNet [11]. We first compare our results with state-of-the-art baselines [10, 17, 29] to show its efficacy. After that, we conduct ablation studies to evaluate different aspects of our proposed method. We then assess the rotational robustness of GMConv. Finally, we analyze how the performance is improved by visualizing the attention maps and RFs of GMConv.

### 4.1. Implement Details

We implement our approach using the publicly available PyTorch framework [26]. We generally replace the first convolution with D-GMConv and the remaining convolutions with S-GMConv to obtain the corresponding GMConv network. Each baseline network architecture and its GMConv counterpart are trained from scratch with identical optimization schemes.

**CIFAR-10 and CIFAR-100.** CIFAR-10 and CIFAR-100 datasets consist of 50k training and 10k test  $32 \times 32$  color images, labeled with 10 and 100 classes, respectively [16]. We evaluate ResNet-20, ResNet-56, and ResNet-18 [10] on the CIFAR datasets [16]. We take random crops from the image padded by 4 pixels on each side for data augmentation and do horizontal flips. We train all the networks with an initial learning rate of 0.1, and a batch size of 128, using an SGD optimizer with a momentum of 0.9. For ResNet-20 and ResNet-56, following the original training strategy [10], we set their weight decay to  $1e^{-4}$ , and divided the learning rate at epochs 80 and 120, with a total of 160 epochs. For ResNet-18, following Cutout [4], the weight decay is set to  $5e^{-4}$ , and the learning rate is divided by 5 at epochs 60, 120 and 160, with a total of 200 epochs.

**ImageNet.** We adopt GMConv to AlexNet [17], ResNet-18, ResNet-50 [10], and MobileNetV2 [29] on the ImageNet dataset [11], which consists of 1.28 million training images and 50K validation images from 1,000 different classes. We use the same data augmentation scheme and training strategies as in [10, 38] for training and apply a

Table 1. Comparisons on CIFAR datasets. We integrate the experiments of Section 4.2 and Section 4.3 into this table.

Model	Method	Params (M)	FLOPs (M)	CIFAR-10 Acc. (%)	CIFAR-100 Acc. (%)
ResNet-20	StdConv			91.58	67.03
	S-GMConv	0.27	42	<b>91.85</b>	<b>67.67</b>
	GMConv			91.81	67.45
ResNet-56	StdConv			92.86	69.84
	S-GMConv	0.85	128	93.16	70.64
	GMConv			<b>93.28</b>	<b>70.65</b>
ResNet-18	StdConv			95.14	77.78
	S-GMConv	11.22	558	<b>95.36</b>	78.03
	GMConv			<b>95.36</b>	<b>78.17</b>

Table 2. Comparisons on ImageNet. We integrate the experiments of Section 4.2 and Section 4.3 into this table.

Model	Method	Params (M)	FLOPs (G)	Top-1 (%)	Top-5 (%)
MobileNetV2	StdConv			71.61	90.40
	S-GMConv	3.50	0.327	71.51	90.24
	GMConv			<b>71.77</b>	<b>90.29</b>
ResNet-18	StdConv			69.77	89.17
	S-GMConv	11.69	1.82	<b>70.32</b>	<b>89.41</b>
	GMConv			69.97	89.22
ResNet-50	StdConv			75.55	92.65
	S-GMConv	25.56	4.13	75.85	92.72
	GMConv			<b>76.40</b>	<b>93.04</b>
AlexNet	StdConv			56.40	79.24
	S-GMConv	61.10	0.714	57.22	79.63
	GMConv			<b>57.38</b>	<b>79.68</b>

single-crop evaluation with the size of  $224 \times 224$  at test time. We train the above models based on the configuration from the origin paper [10] or the samples from PyTorch [26]. By default, we all train the networks with a batch size of 256, using an SGD optimizer with a momentum of 0.9 and a weight decay of  $4e^{-5}$ . For MobileNetV2, the learning rate is initialized to 0.01, multiplied by 0.98 every epoch with a total epoch of 300. For AlexNet, the learning rate is initialized to 0.01, divided by 10 at epochs 30 and 60, with a total of 90 epochs. For ResNets, the learning rate is initialized to 0.1, divided by 10 after every 30 epoch with a total of 90 epochs.

### 4.2. Image Classification Results

In the following experiments, we typically denote the standard convolution as StdConv, the static GMConv as S-GMConv, and the combination of D-GMConv and S-GMConv as GMConv.



**Results on CIFARs.** We evaluate our methods on ResNet-20, ResNet-56, and ResNet-18. We ran each experiment three times and report the average accuracy. The performances of each baseline and its GMConv counterpart on CIFAR-10 and CIFAR-100 are shown in Table 1. The S-GMConv-related models are later discussed in Section 4.3. We can observe that the baseline model and its GMConv counterpart have the same parameters and FLOPs. This is because the extra computational cost of GMConv is mainly from the operation of masking filters on the stem layers, which is eliminated by integrating the mask into the kernel weights after training. Besides, the dynamic GMConv accounts for a small percentage of the whole network, which hardly burdens the capacity and complexity of the network. In such cases, the GMConv variants perform comparably to the baselines and enhance the performance of various models by a clear margin.

**Results on ImageNet.** Table 2 summarizes the results on ImageNet. Similar to CIFAR, the baseline model and its GMConv counterpart have the same parameters and FLOPs. In addition, the Top-1 accuracy of MobileNetV2, ResNet-18, ResNet-50, and AlexNet increases from 0.16%, 0.2% to 0.85% and 0.98% as the model capacity increases, especially for the large kernel network, AlexNet, that employs  $11 \times 11$  and  $5 \times 5$  convolutional kernels. It looks like GMConv is more favorable in large CNNs, especially those employing large convolutional kernels.

### 4.3. Ablation Analysis

In this subsection, we conduct a series of ablation studies to evaluate different aspects of our proposed GMConv method and empirically discuss the key factors of our design. The experimental settings are the same as in Section 4.1.

**Analysis of Static GMConv.** Tables 1 and 2 show the results of pure static GMConv variants, denoted as S-GMConv, on CIFAR datasets and ImageNet. We can observe that simply replacing the convolution CNNs with S-GMConv can improve the performance of most benchmark models on CIFAR datasets and ImageNet. This suggests that allowing the convolution kernel to adjust its receptive field is beneficial for most networks. MobileNetV2 is the only exception within the whole experiment. We hypothesize that it might be because the entire MobileNetV2 adopts  $3 \times 3$  small convolution kernels. And as we will see later in the visualization of the S-GMConv networks, S-GMConv will shrink the receptive field of the first few convolutions, while the receptive field of a  $3 \times 3$  kernel is small enough. In addition, we find that the Top-1 accuracy of S-GMConv ResNet-18 is noticeably higher than the baseline and the GMConv variant. The phenomenon also appears in some CNN architectures on CIFAR datasets, but not so clearly. It seems that small networks cannot effectively build the

Table 3. Comparison of different D-GMConv structures on ImageNet.

Model	Method	#sigma	Pred pattern	Top-1(%)
Resnet-18	StdConv	–	–	69.77
	GMConv	1	$\sigma$	69.95
	GMConv	2	$\sigma_1, \sigma_2$	69.86
	GMConv	2	$\sigma_1, r_\sigma$	<b>69.97</b>
Resnet-50	StdConv	–	–	75.55
	GMConv	1	$\sigma$	76.02
	GMConv	2	$\sigma_1, \sigma_2$	75.84
	GMConv	2	$\sigma_1, r_\sigma$	<b>76.40</b>
AlexNet	StdConv	–	–	56.40
	GMConv	1	$\sigma$	57.06
	GMConv	2	$\sigma_1, \sigma_2$	57.07
	GMConv	2	$\sigma_1, r_\sigma$	<b>57.38</b>

learnable sigma module. We don't put the results of the pure static GMConv variant because it is difficult to converge and get a reasonable accuracy.

**Analysis of Initial  $\sigma$  in S-GMConv.** According to the discussion in Section 3, we know that  $\sigma$  controls the receptive field of the convolutional kernels. The higher the value of  $\sigma$ , the larger the receptive field. Therefore, by adjusting the initial  $\sigma$  value, we can analyze the effect of different initial receptive fields. We compare three initial  $\sigma$  values, 1, 5 and 10, on CIFAR-10 and CIFAR-100. We train ResNet-20, ResNet-56, ResNet-18 and their S-GMConv variants three times to get the average accuracy. Figure 6 provide the comparisons on CIFAR-10 and CIFAR-100. On CIFAR-10, the networks seem to prefer a small initial receptive field, while on CIFAR-100, either too small or too large initial receptive fields may compromise the performance of the networks to some extent. It demonstrates the importance of a suitable receptive field for models. A proper initial receptive field can further improve the performance, whereas too small or too large receptive fields may harm the models. The other side also suggests that 5 is an appropriate initial receptive field value, which can steadily improve the model performance compared with other values.

**Designs of D-GMConv.** We design our learnable sigma module to predict the mask generation parameters. The number and significance of the predicted parameters vary according to the required amount of sigma and the relationship between multiple parameters. If the module predicts only one value, then this value is unquestionably the magnitude of  $\sigma$ , denoted as  $\sigma$ . If the network predicts two values, their meanings can be the magnitudes of  $\sigma_1$  and  $\sigma_2$ , denoted as  $(\sigma_1, \sigma_2)$ , or the magnitude of  $\sigma_1$  and the scale factor  $r_\sigma$ , denoted as  $(\sigma_1, r_\sigma)$ . As shown in Table 3, in general, if the models just predict the magnitude of  $\sigma$  or  $\sigma_1, \sigma_2$ , predicting more sigma parameters does not make the convolution ben-

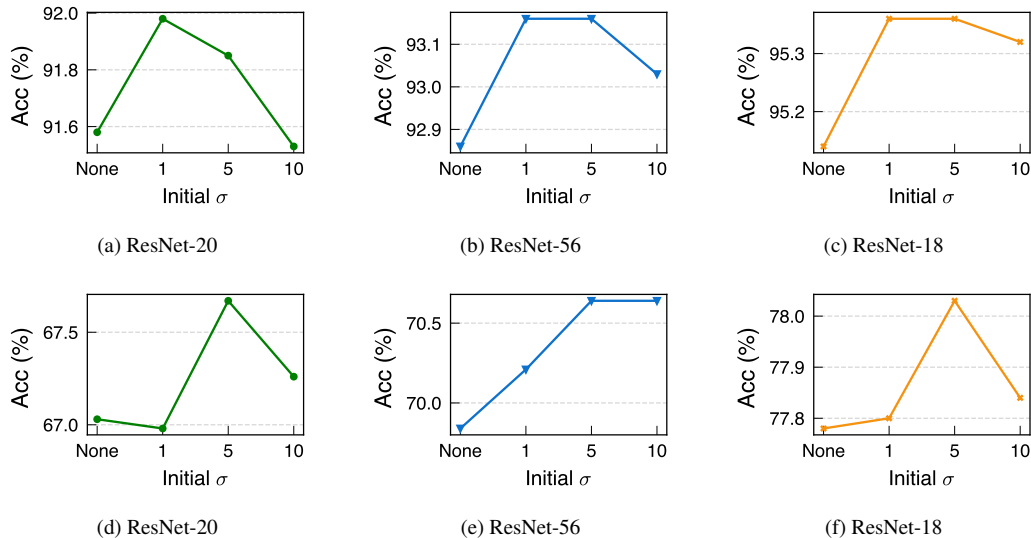


Figure 6. Comparisons of S-GMConv with different initial  $\sigma$  values on (a), (b), (c) for CIFAR-10 and (d), (e), (f) for CIFAR-100. The “None” term refers to the corresponding standard convolution of ConvNets.

efit from a more flexible RF mask. On the contrary, with one predicted parameter  $\sigma$ , the resulting models perform better. However, it does not imply that the elliptical RF mask is inferior to the circular RF mask. Observably, the performance of the two-parameter ( $\sigma_1, \sigma_2$ ) pattern can be improved by predicting  $\sigma_1$  and the correlation ( $r_\sigma$ ) between the two sigmas, where  $\sigma_2$  can be calculated by  $\sigma_1 \times r_\sigma$ . The above experiments demonstrate the effectiveness of our D-GMConv. On the other hand, it also shows that a simple modification to the stem convolution can considerably impact the overall network. In addition, despite the small proportion of the stem layer in CNNs, the design of the stem layer is still necessary.

#### 4.4. Rotation Robustness Analysis

The Gaussian mask will make the convolution concentrate more on the center of the view and suppress the influence of the edge. Considering this, we hypothesize that GMConv may enhance the model’s robustness to rotational distortions.

We then test the trained AlexNets with rotationally distorted images from ImageNet validation set. Table 4 shows the results of different AlexNet variants equipped with standard convolution, GMConv, and S-GMConv, respectively. As can be seen, models equipped with GMConv or S-GMConv achieve higher accuracy than the baseline in all distortions, although all models suffer from the domain shift. For example, on  $45^\circ$  rotated inputs, their accuracies are 1.29% and 2.16% higher than the baseline, respectively. On the other hand, the S-GMConv variant shows stronger robustness than the GMConv. In all distortions, its accu-

acies are higher than the GMConv variant. This is probably because all convolutions in the S-GMConv variant share a circular concentric RF, whereas the GMConv variant introduces an elliptical RF in the first layer; thus, the S-GMConv variant shows superior symmetry to the GMConv variant. In summary, we have demonstrated that GMConv, especially S-GMConv, can enhance the model’s robustness against rotational distortions by an observable margin. Though it may not be the primary reason for GMConv’s effectiveness, we believe it has the potential to inspire future research on the rotational invariance problem.

#### 4.5. Visualization

**Attention Map Visualization.** To show why the proposed GMConv benefits CNNs, we apply the Grad-CAM [30] to visualize the attention maps of ResNet-50 with different convolutions. As shown in Figure 7, one can observe that the integration of S-GMConv can assist networks in better differentiating between the foreground and background, and further introduced GMConv can provide more precise foreground object locating. Additionally, standard convolution usually focuses on a small key part of the target while GMConv could take into account the overall information of the target.

**RF Mask Visualization.** To investigate the effect of RF masks on the network, we visualize in Figure 8 the RF masks of different layers for S-GMConv CNNs. It can be observed that the S-GMConv generally affects the receptive field of the shallow layers of CNN, especially for large convolutional kernels, while in the deep layers, the RFs are not much different from the standard convolution.

Table 4. Top-1 accuracy (%) of AlexNet with different convolutions and rotational distortions on ImageNet.

Method	Rotate 0°	Rotate 45°	Rotate 90°	Rotate 135°	Rotate 180°	Up-down flip
StdConv	56.40	21.69	28.01	12.92	30.17	29.92
S-GMConv	57.22	23.85	29.52	14.80	31.86	31.78
GMConv	57.38	22.98	29.24	13.90	31.48	31.49

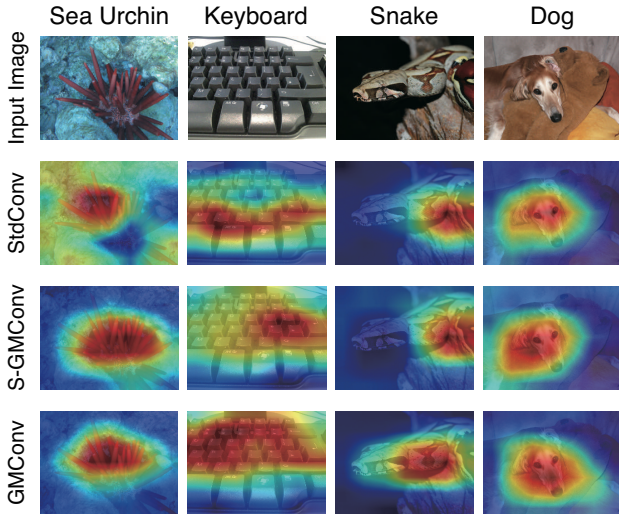


Figure 7. Visualization of attention maps generated by Grad-CAM [30]. We compare the visualization results of ResNet-50 with standard convolutions, S-GMConv, and GMConv. The Grad-CAM visualization is calculated by the last convolutional outputs.

Such visualization suggests that the RF masks may be useful for processing fine-grained information, such as edges, colors, and textures in shallow layers, but not very helpful in processing the context information in deep layers. It suggest that we can focus more on the design of the convolutions in the shallow layers and still retain the standard convolution in the deep layers of the network in the futuer work.

## 5. Conclusion

Inspired by the Gaussian distribution of effective receptive field in CNNs, we propose the Gaussian Mask Convolutional Kernel (GMConv) to introduce a concentric receptive field to convolutional kernels. Existing related works mainly focus on sampling pixels with offsets, which can not model the effective receptive field. In contrast, GMConv modifies the Gaussian function to generate receptive field masks which then are put over the convolutional kernels to adjust receptive fields inside the kernel. In particular, we provide a static version and a dynamic version of GMConv that work on different layers of the network to achieve

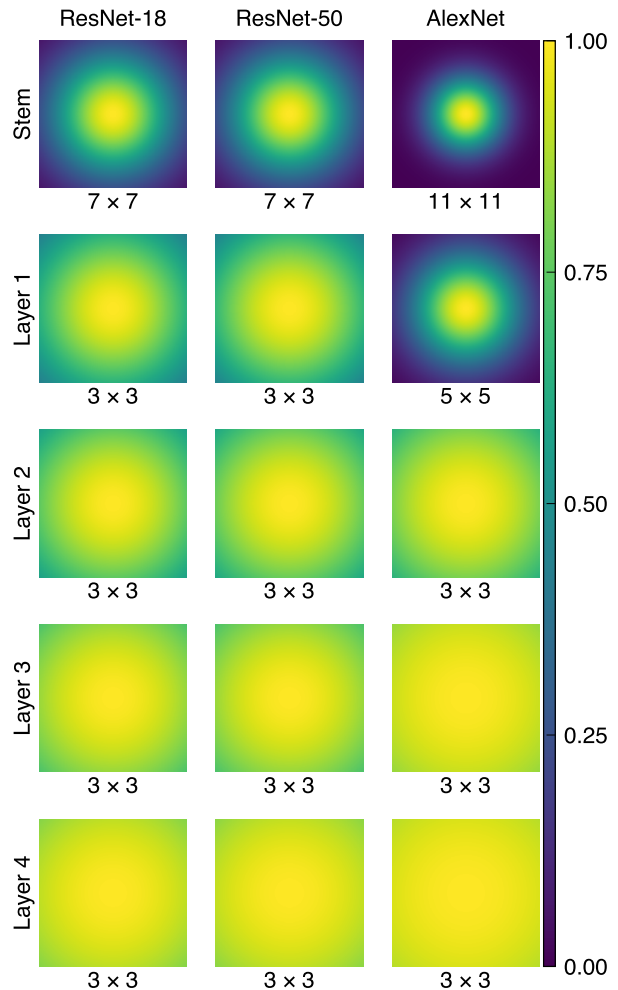


Figure 8. RF masks visualization of S-GMConv networks. We visualize the RF masks of different layer convolutions in ResNet-18, ResNet-50 and AlexNet. In particular, we calculate the average RF masks of ResNet-18, ResNet-50, AlexNet in different body layers.

a good trade-off between effectiveness and complexity. Our GMConv can be easily integrated into existing CNN architectures. Experiments on CIFAR-10, CIFAR-100 and ImageNet benchmark datasets demonstrate that GMConv can substantially boost the performance of equivalent networks. The visualization shows that our GMConv mainly takes ef-



fects on shallow layers, which may suggest possible future applications to CNNs.

## References

- [1] Yinpeng Chen, Xiyang Dai, Mengchen Liu, Dongdong Chen, Lu Yuan, and Zicheng Liu. Dynamic convolution: Attention over convolution kernels. In *Proceedings of the IEEE/CVF Conference on Computer Vision and Pattern Recognition*, pages 11030–11039, 2020. 3
- [2] François Chollet. Xception: Deep learning with depthwise separable convolutions. In *Proceedings of the IEEE Conference on Computer Vision and Pattern Recognition*, pages 1251–1258, 2017. 2
- [3] Jifeng Dai, Haozhi Qi, Yuwen Xiong, Yi Li, Guodong Zhang, Han Hu, and Yichen Wei. Deformable convolutional networks. In *Proceedings of the IEEE/CVF International Conference on Computer Vision*, pages 764–773, 2017. 1, 2, 3
- [4] Terrance DeVries and Graham W Taylor. Improved regularization of convolutional neural networks with cutout. *arXiv preprint arXiv:1708.04552*, 2017. 5
- [5] Xiaohan Ding, Xiangyu Zhang, Jungong Han, and Guiguang Ding. Scaling up your kernels to 31x31: Revisiting large kernel design in cnns. In *Proceedings of the IEEE Conference on Computer Vision and Pattern Recognition*, pages 11963–11975, 2022. 1
- [6] Alexey Dosovitskiy, Lucas Beyer, Alexander Kolesnikov, Dirk Weissenborn, Xiaohua Zhai, Thomas Unterthiner, Mostafa Dehghani, Matthias Minderer, Georg Heigold, Sylvain Gelly, Jakob Uszkoreit, and Neil Houlsby. An image is worth 16x16 words: Transformers for image recognition at scale. *ICLR*, 2021. 1
- [7] Hang Gao, Xizhou Zhu, Stephen Lin, and Jifeng Dai. Deformable kernels: Adapting effective receptive fields for object deformation. In *8th International Conference on Learning Representations, ICLR 2020, Addis Ababa, Ethiopia, April 26-30, 2020*. OpenReview.net, 2020. 2
- [8] Ross Girshick, Jeff Donahue, Trevor Darrell, and Jitendra Malik. Rich feature hierarchies for accurate object detection and semantic segmentation. In *Proceedings of the IEEE Conference on Computer Vision and Pattern Recognition*, 2014. 1
- [9] Kun He, Chao Li, Yixiao Yang, Gao Huang, and John E. Hopcroft. Integrating circle kernels into convolutional neural networks. *CoRR*, abs/2107.02451, 2021. 1
- [10] Kaiming He, Xiangyu Zhang, Shaoqing Ren, and Jian Sun. Deep residual learning for image recognition. In *Proceedings of the IEEE Conference on Computer Vision and Pattern Recognition*, pages 770–778, 2016. 1, 2, 5
- [11] Geoffrey E Hinton, Alex Krizhevsky, and Ilya Sutskever. Imagenet classification with deep convolutional neural networks. *Advances in Neural Information Processing Systems*, 25(1106-1114):1, 2012. 2, 5
- [12] Andrew G Howard, Menglong Zhu, Bo Chen, Dmitry Kalenichenko, Weijun Wang, Tobias Weyand, Marco Andreetto, and Hartwig Adam. Mobilenets: Efficient convolutional neural networks for mobile vision applications. *arXiv preprint arXiv:1704.04861*, 2017. 2
- [13] Jie Hu, Li Shen, and Gang Sun. Squeeze-and-excitation networks. In *Proceedings of the IEEE Conference on Computer Vision and Pattern Recognition*, 2018. 1, 2, 3
- [14] Ajay Jain, Pieter Abbeel, and Deepak Pathak. Locally masked convolution for autoregressive models. In *Conference on Uncertainty in Artificial Intelligence*, pages 1358–1367. PMLR, 2020. 2
- [15] Yunho Jeon and Junmo Kim. Active convolution: Learning the shape of convolution for image classification. In *Proceedings of the IEEE Conference on Computer Vision and Pattern Recognition*, pages 4201–4209, 2017. 1, 2, 3
- [16] Alex Krizhevsky, Geoffrey Hinton, et al. Learning multiple layers of features from tiny images. 2009. 2, 5
- [17] Alex Krizhevsky, Ilya Sutskever, and Geoffrey E Hinton. Imagenet classification with deep convolutional neural networks. In F. Pereira, C.J. Burges, L. Bottou, and K.Q. Weinberger, editors, *Advances in Neural Information Processing Systems*, volume 25. Curran Associates, Inc., 2012. 1, 2, 5
- [18] Alexander Krull, Tim-Oliver Buchholz, and Florian Jug. Noise2void-learning denoising from single noisy images. In *Proceedings of the IEEE Conference on Computer Vision and Pattern Recognition*, pages 2129–2137, 2019. 2
- [19] Shiwei Liu, Tianlong Chen, Xiaohan Chen, Xuxi Chen, Qiao Xiao, Boqian Wu, Mykola Pechenizkiy, Decebal Mocanu, and Zhangyang Wang. More convnets in the 2020s: Scaling up kernels beyond 51x51 using sparsity. *arXiv preprint arXiv:2207.03620*, 2022. 1
- [20] Ze Liu, Han Hu, Yutong Lin, Zhuliang Yao, Zhenda Xie, Yixuan Wei, Jia Ning, Yue Cao, Zheng Zhang, Li Dong, Furu Wei, and Baining Guo. Swin transformer v2: Scaling up capacity and resolution. In *Proceedings of the IEEE Conference on Computer Vision and Pattern Recognition*, 2022. 1
- [21] Ze Liu, Yutong Lin, Yue Cao, Han Hu, Yixuan Wei, Zheng Zhang, Stephen Lin, and Baining Guo. Swin transformer: Hierarchical vision transformer using shifted windows. In *Proceedings of the IEEE/CVF International Conference on Computer Vision*, 2021. 1
- [22] Zhuang Liu, Hanzi Mao, Chao-Yuan Wu, Christoph Feichtenhofer, Trevor Darrell, and Saining Xie. A convnet for the 2020s. In *Proceedings of the IEEE Conference on Computer Vision and Pattern Recognition*, pages 11976–11986, 2022. 1
- [23] Zhichao Lu, Vivek Rathod, Ronny Votel, and Jonathan Huang. Retinatrack: Online single stage joint detection and tracking. In *Proceedings of the IEEE Conference on Computer Vision and Pattern Recognition*, pages 14668–14678, 2020. 1
- [24] Wenjie Luo, Yujia Li, Raquel Urtasun, and Richard Zemel. Understanding the effective receptive field in deep convolutional neural networks. *Advances in Neural Information Processing Systems*, 29, 2016. 1, 3
- [25] Xuezhe Ma, Xiang Kong, Shanghang Zhang, and Eduard Hovy. Macow: Masked convolutional generative flow. *Advances in Neural Information Processing Systems*, 32, 2019. 2

- [26] Adam Paszke, Sam Gross, Soumith Chintala, Gregory Chanan, Edward Yang, Zachary DeVito, Zeming Lin, Alban Desmaison, Luca Antiga, and Adam Lerer. Automatic differentiation in pytorch. 2017. [5](#)
- [27] Ilija Radosavovic, Raj Prateek Kosaraju, Ross Girshick, Kaiming He, and Piotr Dollár. Designing network design spaces. In *Proceedings of the IEEE Conference on Computer Vision and Pattern Recognition*, pages 10428–10436, 2020. [1](#), [2](#)
- [28] Shaoqing Ren, Kaiming He, Ross Girshick, and Jian Sun. Faster R-CNN: Towards real-time object detection with region proposal networks. In *Advances in Neural Information Processing Systems*, 2015. [1](#)
- [29] Mark Sandler, Andrew Howard, Menglong Zhu, Andrey Zhmoginov, and Liang-Chieh Chen. Mobilenetv2: Inverted residuals and linear bottlenecks. In *Proceedings of the IEEE Conference on Computer Vision and Pattern Recognition*, pages 4510–4520, 2018. [5](#)
- [30] Ramprasaath R Selvaraju, Michael Cogswell, Abhishek Das, Ramakrishna Vedantam, Devi Parikh, and Dhruv Batra. Grad-cam: Visual explanations from deep networks via gradient-based localization. In *Proceedings of the IEEE/CVF International Conference on Computer Vision*, pages 618–626, 2017. [7](#), [8](#)
- [31] Evan Shelhamer, Dequan Wang, and Trevor Darrell. Efficient receptive field learning by dynamic gaussian structure. 2019. [3](#)
- [32] Karen Simonyan and Andrew Zisserman. Very deep convolutional networks for large-scale image recognition. *arXiv preprint arXiv:1409.1556*, 2014. [2](#)
- [33] Ke Sun, Bin Xiao, Dong Liu, and Jingdong Wang. Deep high-resolution representation learning for human pose estimation. In *Proceedings of the IEEE Conference on Computer Vision and Pattern Recognition*, 2019. [1](#)
- [34] Xin Sun, Changrui Chen, Xiaorui Wang, Junyu Dong, Huiyu Zhou, and Sheng Chen. Gaussian dynamic convolution for efficient single-image segmentation. *IEEE Transactions on Circuits and Systems for Video Technology*, 32(5):2937–2948, 2021. [3](#)
- [35] Christian Szegedy, Wei Liu, Yangqing Jia, Pierre Sermanet, Scott Reed, Dragomir Anguelov, Dumitru Erhan, Vincent Vanhoucke, and Andrew Rabinovich. Going deeper with convolutions. In *Proceedings of the IEEE Conference on Computer Vision and Pattern Recognition*, pages 1–9, 2015. [1](#)
- [36] Mingxing Tan and Quoc Le. Efficientnet: Rethinking model scaling for convolutional neural networks. In *International Conference on Machine Learning*, pages 6105–6114. PMLR, 2019. [2](#)
- [37] Wenhai Wang, Enze Xie, Xiang Li, Deng-Ping Fan, Kaitao Song, Ding Liang, Tong Lu, Ping Luo, and Ling Shao. Pyramid vision transformer: A versatile backbone for dense prediction without convolutions. In *Proceedings of the IEEE/CVF International Conference on Computer Vision*, pages 568–578, 2021. [1](#)
- [38] Sanghyun Woo, Jongchan Park, Joon-Young Lee, and In So Kweon. Cbam: Convolutional block attention module. In *Proceedings of the European Conference on Computer Vision*, pages 3–19, 2018. [3](#), [5](#)
- [39] Saining Xie, Ross Girshick, Piotr Dollár, Zhuowen Tu, and Kaiming He. Aggregated residual transformations for deep neural networks. In *Proceedings of the IEEE Conference on Computer Vision and Pattern Recognition*, pages 1492–1500, 2017. [1](#), [2](#)
- [40] Brandon Yang, Gabriel Bender, Quoc V Le, and Jiquan Ngiam. Condconv: Conditionally parameterized convolutions for efficient inference. *Advances in Neural Information Processing Systems*, 32, 2019. [3](#)
- [41] Xizhou Zhu, Han Hu, Stephen Lin, and Jifeng Dai. Deformable convnets v2: More deformable, better results. In *Proceedings of the IEEE Conference on Computer Vision and Pattern Recognition*, pages 9308–9316, 2019. [1](#), [2](#), [3](#)